

Chapter 20

Thermal Analysis of Volcanoes Based on 10 Years of ASTER Data on Mt. Etna

Maria Fabrizia Buongiorno, David Pieri, and Malvina Silvestri

Abstract The EOS-1 Terra ASTER (Advanced Spaceborne Thermal Emission and Reflection Radiometer) has acquired about 200 images (100 of them sufficiently cloud-free to be used) over Mt. Etna since 1999. This chapter shows the results from the analysis of 10 years Mt Etna activity using thermal infrared (TIR) high spatial resolution data by a semi-automatic procedure that extracts radiance values of the summit area with the goal of detecting variation related to eruptive events. Night time data showed a good correlation with the main eruptive events that occurred both in the summit and in the flank areas. A comparison of the variance of maximum ASTER TIR radiance with variance of the maximum AVHRR TIR radiance (Advanced Very High Resolution Radiometer) for the same area confirms good correlation in terms of trend and values between the two data sets. Finally this study emphasizes the importance of high spatial resolution TIR data during background monitoring to detect changes in the thermal emission that may be related to an impending eruption and the need to further improve the spatial resolution in the TIR channels to better separate the thermal active areas in volcanic systems.

20.1 Introduction to Current Challenges in Volcano Observation

Using remote sensing techniques to understand the world's volcanoes is a focus of the world's major scientific agencies and space-faring countries (Solomon et al. 2003; USNRC decadal survey 2007). Such emphasis on volcanoes reflects the fact

M.F. Buongiorno (✉) • M. Silvestri
Istituto Nazionale di Geofisica e Vulcanologia (INGV), Rome, Italy
e-mail: Fabrizia.buongiorno@ingv.it

D. Pieri
Jet Propulsion Laboratory, California Institute of Technology, Pasadena, CA, USA

that 500 million people live under the direct threat of volcanic eruptions or their associated environmental effects along with the pursuit of basic earth system scientific information. Warning signs of eruptions, however, are inconsistent and prediction time windows are imprecise and inaccurate. Eruption prediction is a chancy idiosyncratic affair, as volcanoes often manifest waxing and/or waning pre-eruption emission, geodetic, and seismic behavior that is unsystematic. Thus, fundamental to increased prediction accuracy and precision are good and frequent assessments of the time-series behavior of relevant precursor geophysical, geochemical, and geological phenomena, especially when volcanoes become restless.

Signaling the onset of an eruption requires observing the thermal flux of a restless volcano as an important source of information of both persistent low-level thermal activity due to seasonal/diurnal geo-hydrothermal variations, and about rarer anomalous precursor thermal activity (e.g., Pieri and Abrams 2005). To detect such behavior it is important to have knowledge of the thermal activity datum related to a particular volcano in addition to the observation and characterization of its thermal anomaly.

In the past several years there has been progress in using daily 1 km/pixel observations of the Moderate Resolution Imaging Spectroradiometer (MODIS) data. For such data, automated thermal thresholding algorithms are used to detect global thermal anomalies (Wright et al. 2004) and measure volcanic plume and SO₂ gas emissions (Realmuto et al. 1994). Although volcanic thermal features are usually much smaller than a MODIS pixel, these data are capable of showing some sub-pixel thermal anomalies, but typically miss many small subtle thermal anomalies. The Advanced Spaceborne Thermal Emission and Reflection Radiometer (ASTER; Yamaguchi et al. 1998) with multispectral Visible/Near InfraRed (VNIR), Short Wave InfraRed (SWIR) and Thermal InfraRed (TIR) data measured at higher spatial resolution (15, 30 and 90 m, respectively), detects even very small thermal anomalies that are missed by MODIS (Vaughan and Hook 2006). ASTER can point off nadir to view selected targets, such as erupting volcanoes, every few days, thus supplementing the nominal 16 day nadir repeat cycle (Pieri and Abrams 2004).

Here we report on the utilization of ASTER's thermal infrared (TIR) remote sensing capabilities and the Jet Propulsion Laboratory (JPL) ASTER Volcano Archive (AVA) as tools to systematically analyze the spatial and temporal relationships (positively correlated, uncorrelated, and/or negatively correlated) of volcanogenic thermal anomalies and eruptions at Mt. Etna on the Italian island of Sicily. We have examined approximately 200 day and night ASTER images of Mt. Etna with respect to:

1. seasonally biased thermal emission baseline behavior;
2. the form and magnitude of time-dependent thermal emission variability;
3. the limits of spatio-temporal detection of pre-eruption temporal changes in thermal emission in the context of eruption precursor behavior.

Our goal has been to create and analyze a catalog of data by examining the magnitude, frequency, and distribution of Mt. Etna's summit crater thermal signatures at the highest available spatial resolution (90 m/pixel) to exploit one of the largest thermal remote sensing time series of Mt. Etna ever compiled. Further, we demonstrate the value of high spatial resolution TIR time-series data for monitoring significant volcanogenic hazards and risks, especially in the area of thermal precursor activity detection.

Important specific questions inherent in the thermal monitoring of volcanoes are:

- (a) Can eruption precursor phenomena be reliably detected by optical remote sensing techniques?
- (b) What are the spatial, temporal, and spectral intensity relations and detection limits as defined by statistical analyses at high accuracy (e.g., snow vs. cloud mapping for DEM (Digital Elevation Model) creation; low temperature precursor detection; hydrothermal alteration detection);
- (c) How do measurements of relevant time-variable precursors relate among themselves and to overall eruption processes?
- (d) How do such measurements relate to the magnitude, character, and timing of consequent eruptions?
- (e) Are there regional inter-volcano trends in precursor and eruptive phenomena?
- (f) Finally, do the points above relate to the style of volcanism, and can we identify areas where improvement is needed with respect to instrument design or observation strategies?

Systematic global cataloging of volcanic thermal anomalies as measured from high spatial resolution spaceborne sensors is still in its infancy. As the topic matures, it will help to understand the relationships between precursor phenomena and eruptions in the context of global volcanism, as well as in developing a comprehensive observational strategy for spaceborne global monitoring of volcanoes. Moreover, deviations in thermal flux (especially when correlated with gas emissions and surface deformation) may be precursors of changes in the activity state of a volcano, and a subsequent eruption. Nevertheless, eruption forecasting requires both knowledge of the thermal flux data of a given volcanic center and the past relationship between deviations and eruption onset to recognize and rationalize significant change. Ultimately emerging methodologies should and will be refined for applications by the volcanological community to further benefit from presently held and future data sets for active and potentially-active volcanoes.

In particular, such insights and databases will be of use for researchers studying volcanoes that threaten population centers (e.g., Mt. Etna, Mt. Rainier, Mt. Hood, Mt. St. Helens, Vesuvius; the African Rift volcanoes) or air routes (e.g., volcanoes of the Pacific Northwest (Cascades); Indonesian-Philippine archipelagos), especially where volcanoes are not routinely monitored due to the combination of remote location and few resources. Eruption and hazard forecasting for such sites is complicated when there is no sustained local volcanological infrastructure, and when anecdotal reports of volcanic activity conflict. High spatial resolution satellite monitoring

(e.g., ASTER, EO-1) can validate eruption reports, especially where little systematic data exist beyond satellite measurements (Vaughan et al. 2007).

20.2 Theoretical Background of Volcano Monitoring

There is and has been a long and evolving heritage of the spaceborne monitoring of volcanoes. Thermal anomalies associated with volcanic activity with low-resolution weather satellite images were first recognized in the 1960s and 1970s (Gawarecki et al. 1965; Simkin and Kreuger 1977), and subsequent monitoring and analyses progressed from low resolution hot spot detection to more precise and accurate temperature measurements using higher spatial resolution SWIR and TIR data (Lombardo et al. 2006; Ramsey and Dehn 2004). Time-series analyses followed along with techniques for modeling the heterogeneous structure of sub-pixel temperature components (Dozier 1981; Francis and Rothery 1987; Rothery et al. 1988; Crisp and Baloga 1990; Pieri et al. 1990; Oppenheimer 1993; Oppenheimer et al. 1993a, b; Flynn et al. 1994, 2001; Oppenheimer and Francis 1997; Oppenheimer and Yirgu 2002; Wooster and Rothery 1997, 2000; Harris et al. 1997, 1999; Wright et al. 1999, 2000; Lombardo and Buongiorno 2003, 2006; Wright and Flynn 2003; Kaneko and Wooster 2005; Pieri and Abrams 2005; Vaughan et al. 2005, 2007; Vaughan and Hook 2006; Harris and Ripepe 2007).

Currently, for prompt response and hazard mitigation, long time series based on low spatial resolution images (e.g., 250–1,000 m/pixel) with high revisit time are used, as MODIS (Flynn et al. 2002; Wright et al. 2004; Dean et al. 2004; Harris and Ripepe 2007), AVHRR (Harris et al. 1997), GOES (Geostationary Operational Environmental Satellite) (Harris et al. 2001; Pergola et al. 2004), MSG (Meteosat Second Generation) and other weather satellites (Gouhier et al. 2012).

Far fewer studies have utilized higher spatial resolution data (such as ASTER [15 m panchromatic, 30 m multispectral VIS-SWIR, 90 m TIR] or Landsat [30 m multispectral VIS-SWIR, 120 m (MSS, TM) or 60 m (ETM + (Enhanced Thematic Mapper Plus)) TIR]) to obtain more spatially detailed time-series of thermal measurements over volcanoes (Pieri and Buongiorno 1995; Pieri and Abrams 2005; Vaughan and Hook 2006; Ramsey and Dehn 2004). This is because of less frequent observation opportunities of higher spatial resolution ASTER data for a particular volcano due to its smaller swath width and less frequent revisit as compared to the weather satellites. Therefore, an increased probability of obscuration by cloud cover exists. However, since the launch of ASTER in December 1999, 140,000+ images of volcanoes have been acquired worldwide with a number of volcanoes seen frequently enough with ASTER at acceptable cloud coverage. Thus, useful times series data analyses can be undertaken. For instance, one such analysis (Pieri and Abrams 2005) detected winter-time summit crater meltwater in advance of an early spring eruption by the sub-arctic Chikurachki Volcano in the Kurile Islands. ASTER data are currently the only orbital remote sensing data set which allow the detection of low temperature thermal anomalies smaller than the resolution limit of the coarser spatial resolution, MODIS data.

20.3 Mt. Etna Volcano

20.3.1 Geological Background

Mt Etna is a large basaltic composite volcano near the eastern coast of Sicily. It is located in a complex geodynamic environment characterized by the collision of the African and Eurasian continental lithospheric plates (Fig. 20.1a). The geological history of Mt. Etna is subdivided into four main periods (Branca et al. 2004) starting with early submarine activity dated about 500,000 years back to the mid-Pleistocene, to a stratovolcano phase that began about 60,000 years before present, when the eruptive activity further shifted toward the northwest.

Mt Etna is Europe's largest volcano, rising 3,320 m above sea level and with a volume of $>350 \text{ km}^3$, and one of the most active volcanoes on Earth (in the sense of eruptive deposit volumes "production" and eruption frequency, Fig. 20.1b). It has frequent periods of intermittent to persistent activity in the summit area and major eruptions from new vents on its flanks every 1–20 years. The main feature of Etnean activity is voluminous lava emission with occasionally strong explosive activity that occurs in its current configuration of four summit craters. Some of the eruptions from its flanks also show high degrees of explosivity, such as those in 1669, 1879, and 2002–2003 (as reported in URL 1 and URL 2). Mt. Etna lies near the eastern (Ionian) coast of Sicily and occupies a surface area of around $1,200 \text{ km}^2$ with a perimeter exceeding 135 km. Its summit height varies frequently as a function of eruptive activity or due to minor collapse events at the summit craters. Growth of the summit was concentrated at the Northeast Crater, a feature that was formed in 1911 with nearly constant activity at the crater since the mid-1950s which has led to the growth of a large cone around it. Activity at the Northeast Crater became rather infrequent since the mid-1980s and since then the height of its cone decreased to 3,330 m asl (as measured in 2007). The Southeast Crater which was formed in 1971 has the youngest cone of the four summit craters, and underwent a period of dramatic growth between 1998 and 2001. Within the last 2 years, that growth has continued causing instability of the aggrading growing cone and there have been frequent lava fountains and lava flow eruptions.

Mt. Etna is unique for a number of reasons. First, it has the longest record of historical eruptions among all volcanoes on Earth (Simkin and Siebert 1994; Branca and Del Carlo 2004). Its first historically documented eruption occurred at about 3500 BP, and the total number of documented Mt. Etna eruptions is 209 (18 among them questionable) through late 1993 (Simkin and Siebert 1994). In addition to these aforementioned eruptions, relatively recently spectacular and vigorous summit eruptions have occurred in 1995–2001, flank eruptions in 2001, 2002–2003, 2004–2005, and 2008–2009, plus a period of intermittent summit activity during the period 2006–2011. Over to the last four centuries Mt. Etna has shown a rapid increase of activity also in terms of magma erupted (Fig. 20.1b).

Most magma ascends to the surface through the central conduit system of Etna, which leads to the frequent summit activity. Unless magma ascent is very rapid,

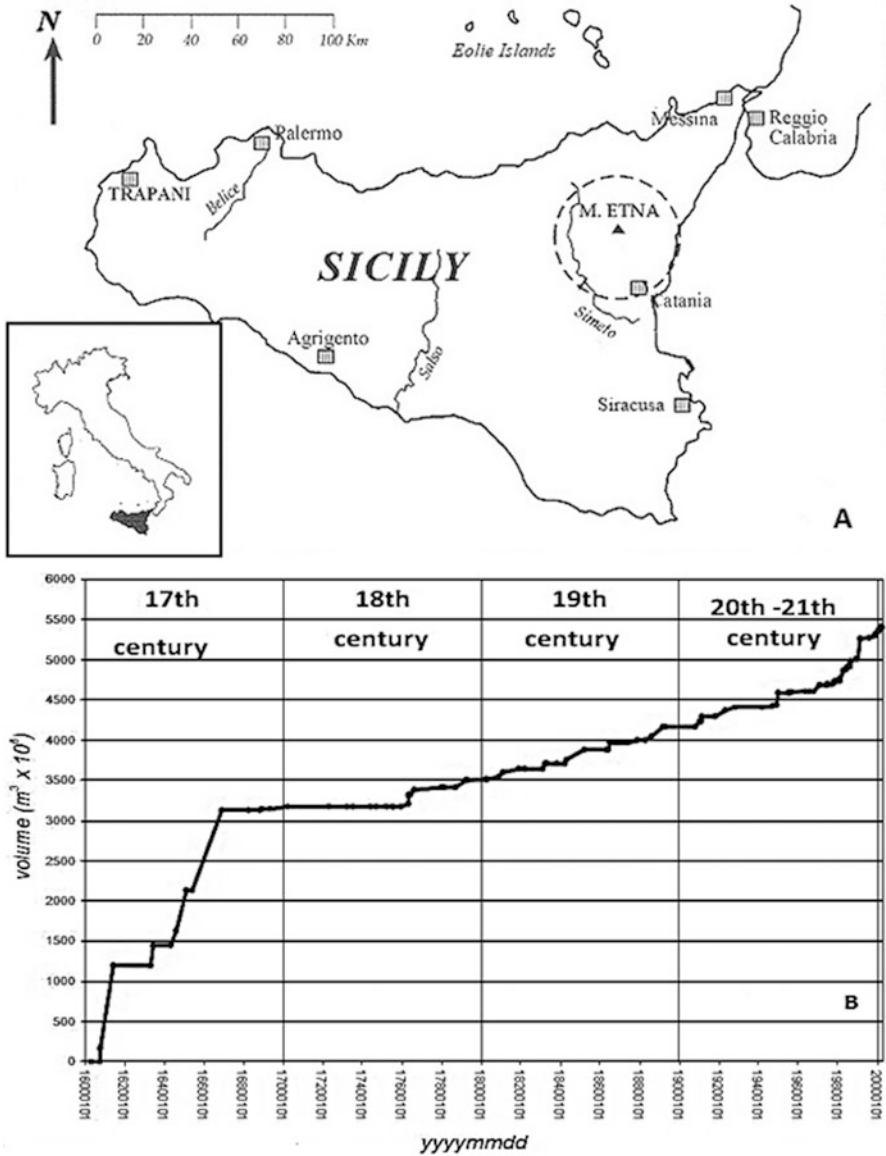


Fig. 20.1 (a) Mt. Etna geographic location; (b) a plot showing the increase of erupted magma volume starting from the end of the eighteenth century and a further increase between the end of the twentieth and the beginning of twenty-first century (Courtesy of Behncke et al. 2005; Neri et al. 2011). Note also the most recent increased rate of magma eruption

much gas is lost from the magma during its ascent to the surface, and significant volumes of relatively gas-poor magma are stored in the shallow plumbing system of the volcano (Fig. 20.2). During many flank eruptions of Etna, such gas-poor magma exits laterally from the central conduits, resulting in relatively weak or almost no

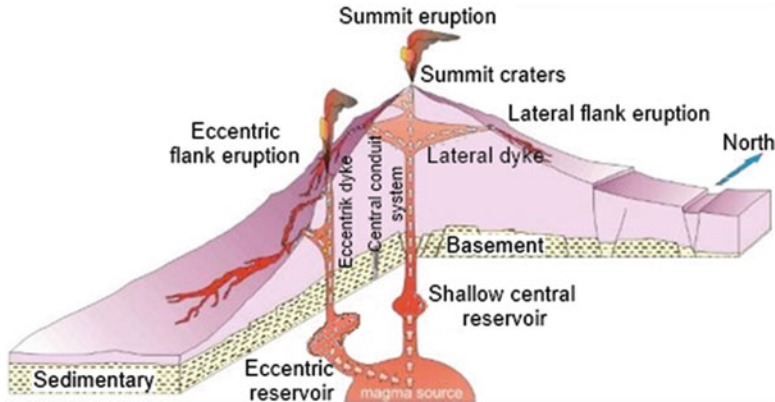


Fig. 20.2 Hypothetical and simplified scheme of the magmatic plumbing system of Etna, illustrating magma transport feeding summit activity and the two different types (lateral vs. eccentric) flank eruptions (Courtesy of Behncke and Neri 2003, edited)

explosive activity but copious lava outflow. Most flank eruptions during the twentieth century were of this type; they are commonly called “lateral” flank eruptions. Typically such eruptions are accompanied by the cessation of summit activity and some collapse at the summit craters, as the central conduit system is drained of magma.

20.3.2 Study Area

Our analysis was focused on the Mt. Etna summit area in order to monitor and detect changes in the thermal emission during both quiescent and eruptive periods (e.g., selected Area of Interest [AOI, rectangle] in inset a of Fig. 20.3). A second area, called “Piano delle Concazze” (inset b of Fig. 20.3) was also selected as a reference background since it is characterized by mineralogically homogeneous terrain composed of fine tephra and ash deposits.

20.4 Available Data and Data Processing

20.4.1 ASTER Thermal Infrared Data Set Acquired Between Year 2000 and 2010

ASTER is one of the five sensors systems on-board the Terra platform launched in December 1999 as part of the NASA Earth Observing System (EOS). ASTER was built by a consortium of the Japanese government, industry, and research groups.

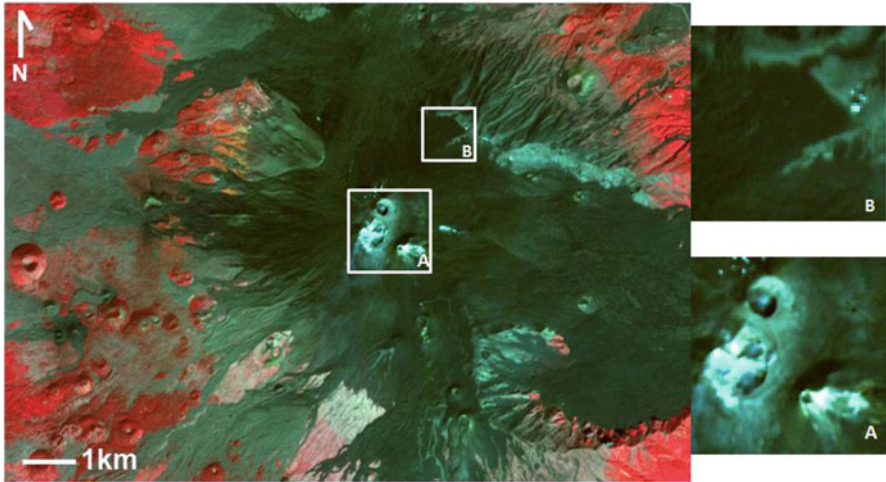


Fig. 20.3 Aster image acquired on 2009, 7th October . Summit craters area and Piano delle Concazze reference area shown on ASTER RGB composite from VIS channels. (a) Selected Area of Interest [AOI, rectangle]: upper left corner = $37^{\circ}44'25.98''$ lat $14^{\circ}59'10.97''$ lon; lower right corner = $37^{\circ}45'43''$ lat $15^{\circ}0'27''$ lon; maximum elevation = 3,330 mASL; 550 pixels in area; (b) AOU center = $37^{\circ}45'53.64''$ lat $14^{\circ}1'9.84''$ lon, elevation = 2,800 mASL, approximately 5 pixels in area

Currently, it is the only known available sensor acquiring images at high spatial resolution in TIR channels (Table 20.1).

Since the launch of the EOS-1 Terra Satellite, images have been acquired over the 10 year period between 2000 and 2010 for Mt Etna area, in Sicily. During this period a number of eruptions have occurred with substantially different intensity and durations. Some occurred at the summit while others occurred on the flanks of Mt. Etna, and several eruptions have manifested as small lava fountains events.

Here we focus on the changes of thermal emission in the summit area of Mt. Etna as analyzed in 200 ASTER images, including 91 daytime and 109 nighttime images. Table 20.2 shows the whole ASTER Mt. Etna data collection reported in terms of number of images per year, broken down with respect to daytime and nighttime acquisitions (e.g. 10:00 AM UTC time and about 21:00 UTC time, respectively).

20.4.2 AVHRR Thermal Infrared Data Set Acquired During the 2006 Eruption

In 2004 INGV established a NOAA-AVHRR (National Oceanic and Atmospheric Administration – Advanced Very High Resolution Radiometer) station, which

Table 20.1 ASTER instrument characteristics (Yamaguchi et al. 1998)

Instrument	VNIR		SWIR		TIR	
Bands and spectral range (μm)	1	0.52–0.60	4	1.60–1.70	10	8.125–8.475
	2	0.63–0.69	5	2.145–2.185	11	8.475–8.825
	3N	0.78–0.86	6	2.185–2.225	12	8.925–9.275
			7	2.235–2.285	13	10.25–10.95
			8	2.295–2.365	14	10.95–11.65
9	2.360–2.430					
Spatial resolution (m)	15		30		90	
Swath width (km)	60		60		60	
Cross track pointing	± 318 km ($\pm 24^\circ$)		± 116 km ($\pm 8.55^\circ$)		± 116 km ($\pm 8.55^\circ$)	
Quantisation (bits)	8		8		12	
Revisit time (days)	16		16		16	

Table 20.2 ASTER data collection during 10 years, daytime and nighttime images and main eruptive events

Year	n. of ASTER images daytime (about 10:00 UTC)	n. of ASTER images nighttime (about 21:00 UTC)	Start main eruptive events	Stop main eruptive events
2000	4	3		
2001	4	13	17 July	9 August
2002	6	21	26 October	
2003	13	12		23 January
2004	15	7	7 September	
2005	4	10		8 March
2006	8	13	14 July	15 December
2007	15	12	4 September	5 September
			23 November	24 November
2008	9	5	13 May	
2009	4	7		4 July
2010	9	6	–	–

consists of a fully integrated antenna tracking and ground station for receipt of AVHRR satellite imagery.

The AVHRR sensor provides imagery in the visible, near infrared and thermal infrared wavelength bands. The NOAA satellites have a circular, polar, sun-synchronous orbit, with an altitude of 850 km and with a period of about 100 min. A sun-synchronous orbit means that each satellite overpass always occurs at the same point at the same local time. For the NOAA satellite constellation, this allows up to ten overpasses per day, depending on the latitude of the volcano target (Table 20.3).

The AVHRR is a radiation-detection imager that can measure the surface emitted/reflected electromagnetic radiation in different bands ranging through visible, near IR and IR wavelengths.

For this work we focus on the changes of thermal emission in the summit area of Mt. Etna as analyzed in 579 overall AVHRR images nighttime starting from 1st June 2006 to 30th November 2006. The result of this analysis will be compared in the next sessions with results obtained by using ASTER data. The 2006 eruption has been chosen for the high availability of ASTER and AVHRR data.

Table 20.3 AVHRR instrument characteristics (from NOAA web site, [URL 3](#))

Instrument	VNIR		MIR-SWIR		TIR	
Bands and spectral range (μm)	1	0.580–0.680	3a	1.580–1.640	4	10.3–11.3
	2	0.725–1.000	3b	3.550–3.930	5	11.5–12.5
Spatial resolution (km)	1.1		1.1		1.1	
Swath width (km)	$\pm 1,447$		1,447		1,447	
Revisit time (considering all NOAA constellation)	Daily (about 7 acquisition per day)		Daily (about 7 acquisition per day)		Daily (about 7 acquisition per day)	

20.4.3 Data Processing: Method

Considering the goal of detecting very small changes in the radiant emission from volcano summit craters, the methodology adopted in this study was based on the analysis of the radiance values measured by the ASTER sensor. We avoided the application of inversion algorithms to calculate the ground temperature, due to its strong dependence on knowledge of the ground emissivity and local atmospheric conditions. The availability of a stable reference background area (“Piano delle Concazze”) very near to the summit crater area permits us to use a statistical approach for a long time series of observations. A goal of this study is to calculate changes in thermal emissions from very well calibrated and geocorrected TIR images to perform a rapid analysis of the thermal behaviour in active volcanic areas where the ground monitoring is not available or insufficient.

The ASTER data product L1B data (i.e., radiance at the sensor) was first separated into daytime and nighttime data, as well as summer and winter acquisitions. The L1B was used because it contains images already resampled to the geometry of the appropriate UTM projection with the WGS84 Datum. In fact the ASTER Level-1B Registered Radiance at the Sensor product contains radiometrically calibrated and geometrically co-registered data for the acquired channels of the three different telescopes of Level-1A data. The Level-1B data set is produced by applying the radiometric calibration and geometric correction coefficients to the Level-1A.

The most suitable data for analyses was extracted based on visual inspection selecting 37 daytime and 65 nighttime cloud free ASTER images. Unfortunately, the relatively infrequent repetition cycle of ASTER’s (i.e., 16 day nadir repeat) and cloud occurrence reduced the number of available ASTER observations for the assessments of volcanologically quiescent and active periods.

For each data set, the maximum radiance, mean radiance and variance were calculated using ASTER’s TIR Band 13 (10.65 μm) that is not affected by SO_2 emissions. This channel was utilized because of the high elevation of the site (e.g., over 3,000 m asl, hence low atmospheric column water vapor and atmospheric correction were not required because in thermal region the aerosol type plays a negligible role because of the long wavelength) and high emissivity in the selected

TIR channel ($\epsilon \sim 0.95$ as measured during field campaigns by means of FTIR (Fourier Transform InfraRed) instrument, model 102F, Fig. 20.4).

All cloud free data have been processed by means of IDL code and ENVI algorithms, implemented in three steps:

- first step: from the original cloud free data format (LIB), the georeferenced images are obtained using ENVI batch command and the radiance at the sensor is automatically produced.
- second step: for each image the selected area has been analyzed extracting maximum, variance and mean according to area reported in the in Fig. 20.3.
- third step (only for AVHRR data processing): for each image, considering the area in the inset a of Fig. 20.3, the pixel containing clouds are rejected. As first approximation, the cloud presence is verified if the brightness temperature is negative (AVHRR channel 4 unit is brightness temperature). Only positive pixels are converted in radiance and used to compute the maximum and the variance.

20.5 Results and Discussion

Data analysis was performed to test our capability to detect the starting phase of an eruptive event using the variation in thermal emissions from thermal active areas (e.g., summit craters or fumaroles fields) as an index. The 10 years of Mt. Etna activity showed a large number of eruptive episodes spanning modalities that included short-lived explosive emissions of lava in fountains, to persistent effusive lava flow events both from summit craters and flank fissures. This high variability volcanic activity modes made it very difficult to consistently detect initial stages of such events using the variation of surface emitted radiance as a criteria. Additionally, the large area of the volcanic structure exhibited a complex overlay of multi-temperature thermal emission sources comprised of previously-erupted-now-cooling materials in close proximity of a new thermal event. To distinguish these different volcanic phases, and understanding of both the spatial and temporal resolutions of satellite sensors plays a very important role. The ASTER's daytime time series data acquired shows high variance in perceived (surface) thermal energy, and the volcanic thermal emission component is not clearly separable from insolation (Fig. 20.5a). In contrast, ASTER's night observations show well defined episodes of increasing thermal emission of summit craters (Fig. 20.5b) because nighttime data generally exhibit a more uniform background temperature that resulted from the low thermal inertia of the porous volcanic surface tephra layer (e.g., intrinsically low Shannon entropy). Thus, we found that the statistical (Gaussian) variance of thermal radiant emissions is able to delineate main eruptive episodes with respect to the maximum geothermally induced radiance, especially for the 2001, 2002, 2006, and 2008 eruptive episodes (Fig. 20.5b). Even if in 2004–2005 an eruption occurred, the variance value is not high enough to delineate the event. For the two 2007 eruption events no ASTER data were available.

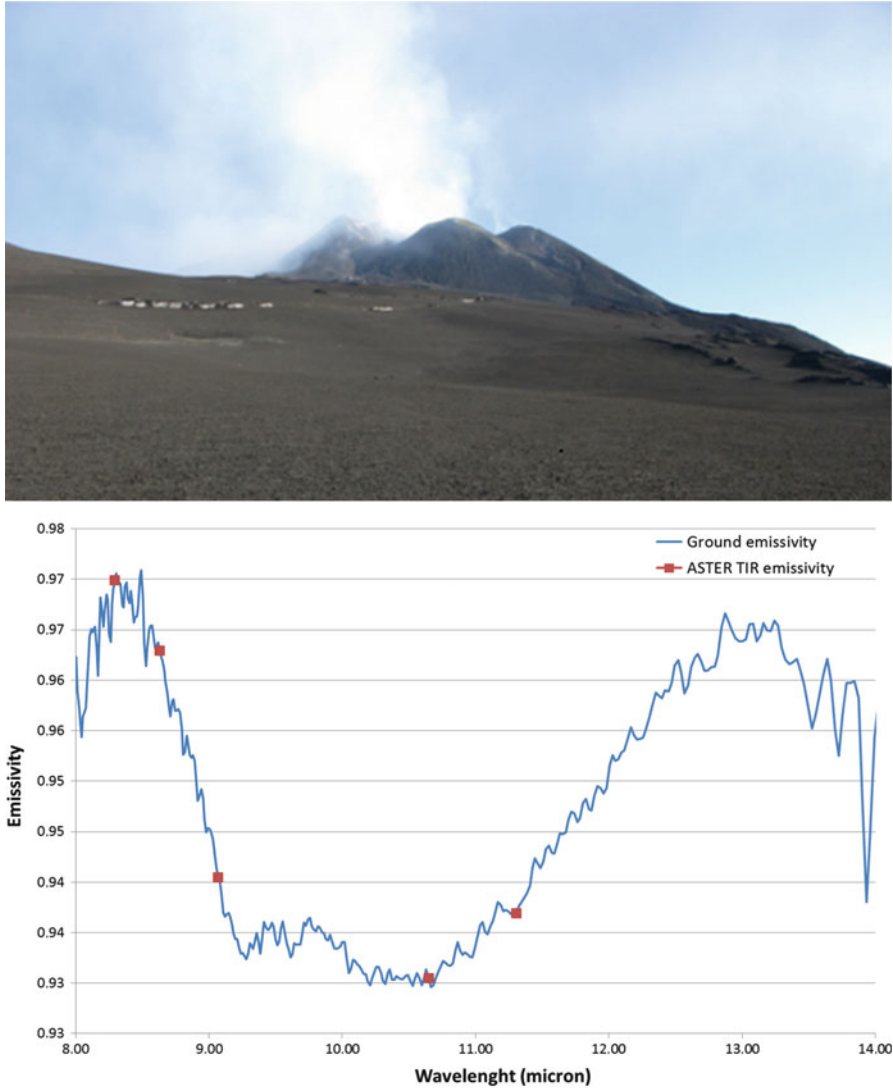


Fig. 20.4 At the *top* Etna summit craters area are shown; on the *bottom*, summit crater scoria/tephra spectral emissivity measured at this site and spectral signature resampled at ASTER TIR wavelengths. The ground emissivity has been measured during field campaigns (2009, 7th October 2009) by means of FTIR (Fourier Transform InfraRed) instrument, model 102F

Particular focus was directed at the 2006 summit eruption which started in July 2006 and showed many different phases although erupting only manifested with two main lava flows (Fig. 20.6). For this eruption, we analyzed the pre-eruptive phase since four night time ASTER TIR images were available. These data show an

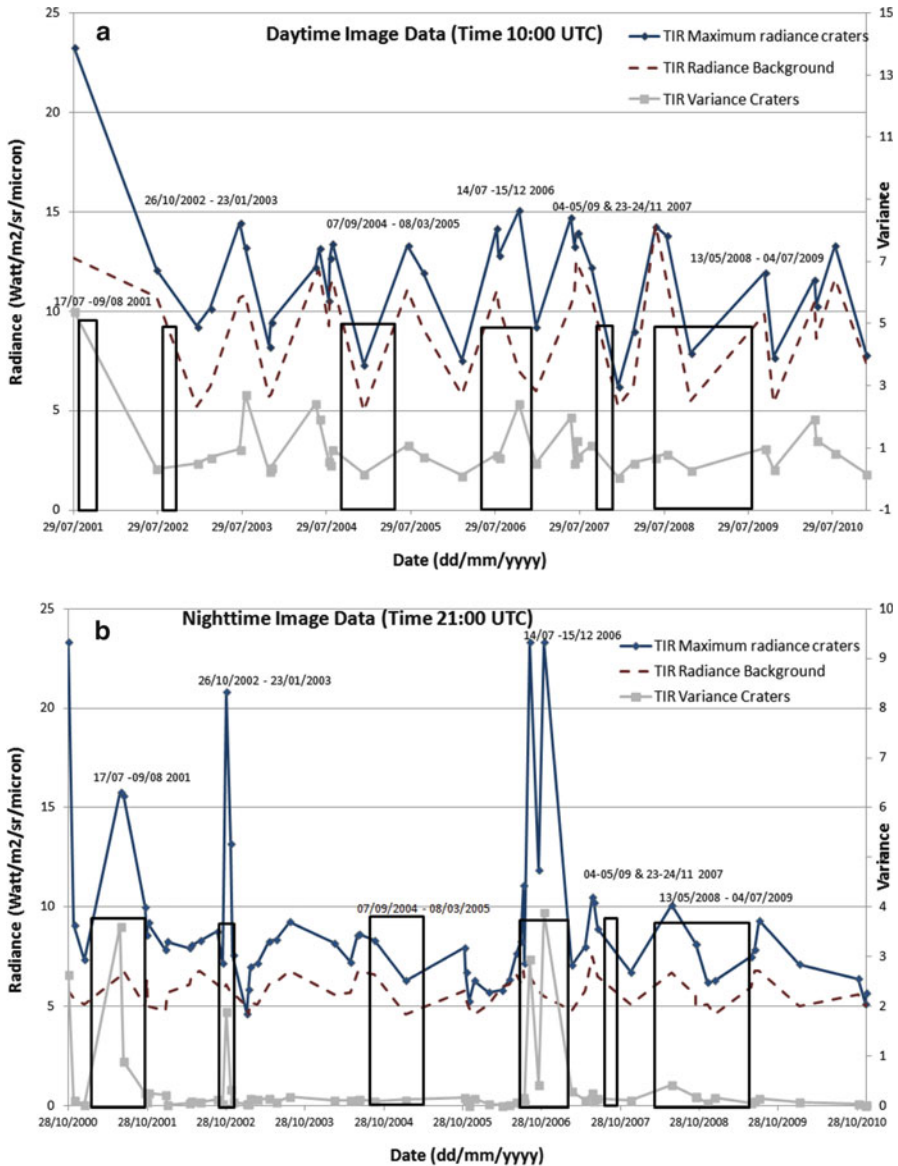


Fig. 20.5 (a) Maximum summit crater radiances for Mt. Etna, derived from ASTER TIR data, along with the statistical variance of radiance and in the designated background area during daytime. (b) Maximum summit crater radiances for Mt. Etna, derived from ASTER TIR data, along with the statistical variance of radiance and in the designated background area for the nighttime observations, showing the increase of thermal energy emission from the summit areas during the 2001, 2002, 2006 and 2008 eruptions. The black line describes for both plots the main eruptive events reported in Table 20.2. For both plots the adimensional variance is reported on the right side of Y axis and the radiance ($\text{Watt/m}^2/\text{sr}/\text{micron}$) on the left Y axis, respectively

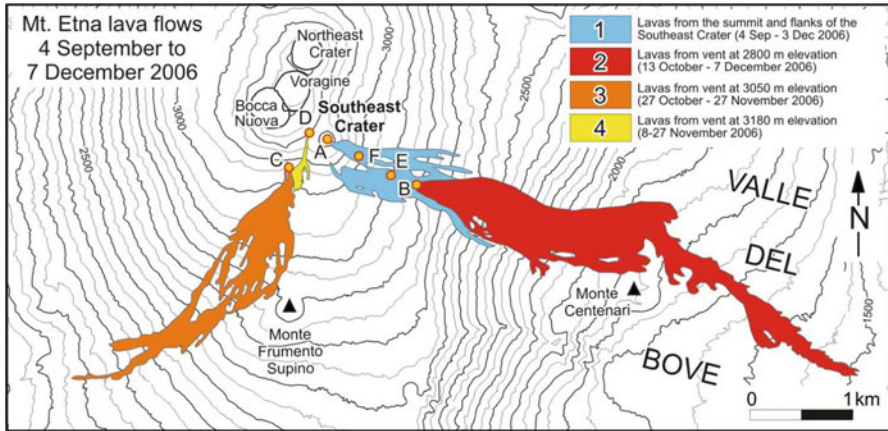


Fig. 20.6 Map of the 2006 lava flow location and extent (Courtesy of Behnke et al. 2008)

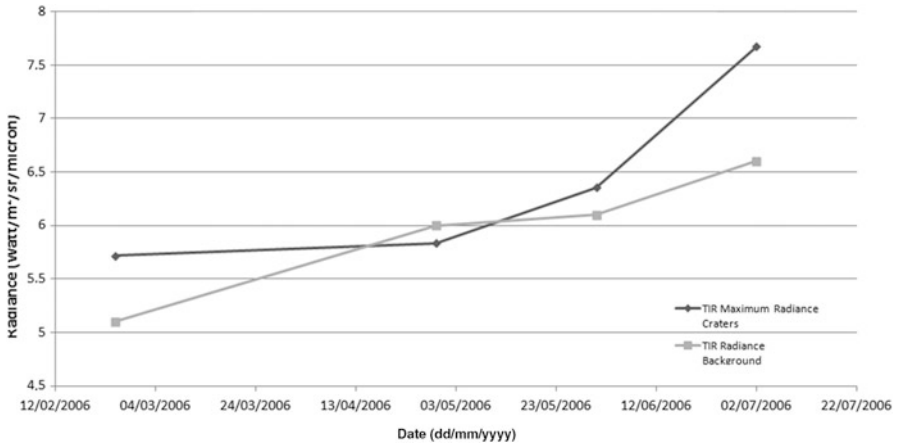


Fig. 20.7 ASTER maximum radiance emitted from summit craters before the beginning of the July 2006 eruption. The value inversion on April 29th 2006 is due to thin clouds present on summit craters which reduce the radiance values compared with the background

increase in the emitted summit crater radiance starting in May 2006 (Fig. 20.7). In the plot of Fig. 20.7 the presence of an higher value of the background respect to the summit crater area is probably due to the presence of scattered thin clouds over the summit crater area which may absorbs part of the emitted radiance toward the sensor for the 29th April 2006 image.

Regrettably, the relatively low frequency of the ASTER data acquisitions (nighttime in particular) did not permit verification of similar pre-eruptive increase in the Mt. Etna summit crater thermal activity for the 2001, 2002 and 2008 eruptions.

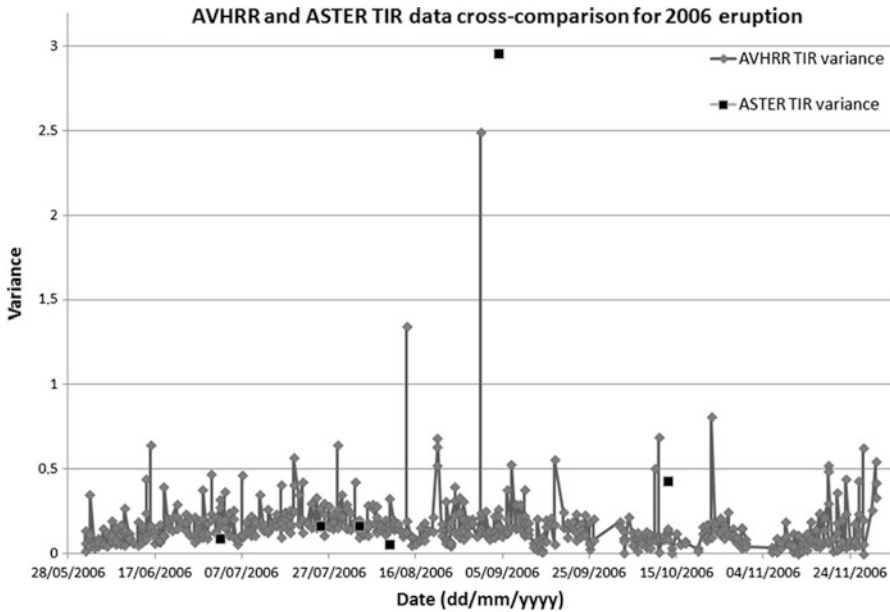


Fig. 20.8 Cross-comparison of variance values obtained by using AVHRR and ASTER data acquired during the 2006 eruption

Finally, the variance of the maximum ASTER TIR radiance during the 2006 eruption was compared with the variance of the maximum AVHRR TIR radiance for the Mt. Etna summit area. Despite the large difference in spatial resolution difference between the two sensors (ASTER = 90 m/pixel, AVHRR = 1,000 m/pixel) and the dimension of the considered area which in AVHRR case covers all parts of the summit of Mt. Etna, the plot in Fig. 20.8 shows a good correlation in terms of trend and values between the two data sets. ASTER data show a higher variance of maximum radiance values than AVHRR data due to the presence of active lava flows. Clearly, the lower spatial resolution of the AVHRR pixels dilutes and smoothes the contribution of emitting pixels in the variance of the radiant intensity, which is resolved at over two orders of magnitude greater spatial resolution in the ASTER TIR data. Even if this comparison shows that AVHRR sensor provides the frequency necessary to detect the onset of large thermal anomalies, its low spatial resolution allows us to detect only very large or very hot anomalies; similarly the ASTER sensor provides information at an improved spatial scale more suitable for scientific analysis, but less useful for a rapid response monitoring systems (Ramsey and Dehn 2004) because of relatively sparse temporal sampling.

20.6 Conclusion

Clearly, the monitoring of thermal features associated with the onset of volcanic eruptions is important for fundamental scientific reasons. Such work has crucial significance for anticipating and mitigating volcanic hazards, not only to people

living in close proximity to volcanic features, but also for those living at long distances from the erupting volcano, but who nevertheless may be affected from related phenomena such as airborne ash hazards.

Recent advances in satellite and airborne remote sensing technologies provide volcanologists with new tools for measuring the thermal emissions of restless volcanoes. In particular, subtle (or not-so-subtle) changes in perceived radiance may be prompt precursors of impending eruptions.

Mt. Etna presents an excellent opportunity for systematic investigation of the potential relationships between changes in thermal radiance and the timing, magnitude, and mode of subsequent eruptive activity because of its current restless state and frequent summit crater activity that is often associated with lava flow extrusions from its summit craters and flanks. In particular, the data record of remote sensing observations provide one of the most comprehensive databases available for volcanoes on Earth. Here especially the Landsat and ASTER earth observation missions are of unprecedented value (e.g., Pieri et al. 1990; Pieri and Buongiorno 1995; Wright et al. 2000; Pieri and Abrams 2004; Lombardo and Buongiorno 2006).

We are now just beginning to mine such data archives and the current insights are preliminary. However, at least a couple of conclusions can be drawn from the results presented here:

1. *For Mt. Etna, the total thermal energy emitted from its summit craters appears to increase before an eruption.* While this may seem intuitive, it is not a guaranteed situation. It is more likely for basaltic volcanoes with fairly open plumbing systems with relatively low viscosity magmas. For volcanoes that are more silicic, and thus have higher viscosity magmas (e.g., Andean volcanoes, such as Lascar), the opposite can be true. This results in the restricted magma ascent in advance of internal pressure build-up and subsequent paroxysmal explosions. This does not seem to be the current pattern at Mt. Etna.
2. *From the remote sensing perspective, an increase in the variance of Mt. Etna summit crater thermal energy output appears to be correlated with the eruption onset.* This tends to be more evident in night time data. However, during an eruption the signal-to-noise ratio (SNR) of summit crater variance to background variance is a factor of five (or more) higher than the SNR of maximum radiance (dependent on measurement of the radiance of single pixel) vs. average background radiance. For data mining applications in newly emerging large time-series data bases this distinction can be significant for automatic eruption detection algorithms.
3. *Volcanic summit crater activity at Mt. Etna is well-characterized at spatial scales of <100 m/pixel and characterized relatively poorly at spatial scales equal to or greater than 1,000 m/pixel for TIR data.* At larger spatial scales, maximum temperatures and variances are diluted and smoothed. In daytime data effects of solar insolation hamper the detection of relevant changes in summit crater radiant emissions, except for very strong precursor activity. This has not

been viewed as a persuasive argument to increase the spatial resolution of new TIR sensors planned for future earth orbital missions in Europe or the United States. However, data and analyses presented here provide concrete evidence of such a monitoring scenario. For volcanoes elsewhere, where observing conditions may not be as optimal (e.g., frequent cloud cover, high humidity, cryo-burdened summits – see Pieri and Abrams 2005) a spatial resolution <100 m/pixel may be critical in detecting thermal precursors.

4. *Frequent temporal sampling is also a crucial component in detecting thermal changes that may precede eruptions, even for very well-posed volcano natural laboratories like Mt. Etna.* Current and recent orbital remote sensing missions in low earth orbit (e.g., ASTER, EO-1, Landsat) have nadir repeat intervals of about 16 days. ASTER with off-nadir pointing can reduce the revisit time up to 3 days but off-nadir view looks are disadvantageous in viewing geometry. Nevertheless, future missions should investigate schemes for increasing temporal sampling at high spatial resolutions (<100 m/pixel) for TIR instruments. Some strategies could include a constellations of satellites (e.g., “cube-sats”) or satellites with much larger instantaneous fields of view. Clearly in the future, such approaches are crucial to improve both our basic knowledge of volcanoes, and our ability to protect property and human life from volcanic hazards.

We also hope that our work will support the development of future multispectral and hyper-spectral airborne (e.g., manned and UAV) and spaceborne imagers by providing a basis for instrument requirements (e.g., spatial and spectral resolution, wavelength range, dynamic range) with respect to volcanogenic thermal anomaly detection as convolved with intrinsic (e.g., flux, intensity, emissivity), and extrinsic (e.g., atmospheric emissions, water vapor, clouds) scene parameters. Such knowledge will also significantly influence the development of data collection strategies (e.g., image swath, repeat time, pointing capability, orbital parameters) to maximize the probability that subtle early low intensity thermal anomalies related to subsequent eruption activity will be effectively detected. We hope that this work will help to guide the development of future airborne (manned/unmanned) and orbital instrumentation for NASA (National Aeronautics and Space Administration), ESA (European Space Agency), ASI (Agenzia Spaziale Italiana), DLR (German Aerospace Center) and others, for prediction and mitigation of volcanic hazards, and in the pursuit of basic knowledge of volcanoes.

Acknowledgments The authors would like to thank US and Japanese colleagues of the ASTER Joint Science Team, the NASA Land Processes Distributed Active Archive Center in Sioux Falls, South Dakota (USA) and the Earth Remote Sensing Data Analysis Center (ERSDAC) in Tokyo (Japan) for cooperation in obtaining and analyzing the ASTER data used for this study, as well as the Japanese Ministry of Economy, Trade and Industry (METI) for its support of the ASTER mission. This work was carried out, in part, at the Jet Propulsion Laboratory (JPL) of the California Institute of Technology under contract to the Science Mission Directorate of NASA. Moreover the authors would like to thank Marco Neri and Boris Behncke working at INGV Mt. Etna Observatory who have provided the Mt. Etna eruption history and maps and Massimo Musacchio working at INGV in Rome for many helpful discussions.

References

- Behncke B, Neri M (2003) The July–August 2001 eruption of Mt. Etna (Sicily). *Bull Volcanol* 65:461–476. doi:[10.1007/s00445-003-0274-1](https://doi.org/10.1007/s00445-003-0274-1)
- Behncke B, Neri M, Nagay A (2005) Lava flow hazard at Mount Etna (Italy): new data from a GIS-based study. In: Manga M, Ventura G (eds) Kinematics and dynamics of lava flows. *Geol Soc Am Spec Pap* 396, pp 187–205. doi:[10.1130/0-8137-2396-5.189](https://doi.org/10.1130/0-8137-2396-5.189)
- Behncke B, Calvari S, Giammanco S, Neri M, Pinkerton H (2008) Pyroclastic density currents resulting from interaction of basaltic magma with hydrothermally altered rock: an example from the 2006 summit eruptions of Mount Etna. *Italy Bull Volcanol* 70:1249–1268. doi:[10.1007/s00445-008-0200-7](https://doi.org/10.1007/s00445-008-0200-7)
- Branca S, Del Carlo P (2004) Eruptions of Mt. Etna during the past 3,200 years: a revised compilation integrating the historical and stratigraphic records. In: Bonaccorso A, Calvari S, Coltelli M, Del Negro C, Falsaperla S (eds) Etna volcano laboratory, Geophysical monograph series 143. AGU, Washington, DC, pp 1–28, 369pp
- Branca S, Coltelli M, Gropelli G (2004) Geological evolution of Etna volcano. In: Bonaccorso A, Calvari S, Coltelli M, Del Negro C, Falsaperla S (eds) Etna volcano laboratory, Geophysical monograph series 143. AGU, Washington, DC, pp 49–63
- Crisp J, Baloga S (1990) A model for lava flows with two thermal components. *J Geophys Res* 95 (B2):1255–1270
- Dean KG, Dehn J, Papp KR, Smith S, Izbekov P, Peterson R, Kearney C, Steffke A (2004) Integrated satellite observation of the 2001 eruption of Mt. Cleveland, Alaska. *J Volcanol Geotherm Res* 135:51–72
- Dozier J (1981) A method for satellite identification of surface temperature fields of subpixel resolution. *Remote Sens Environ* 11:221–229
- Flynn LP, Mouginitis-Mark PJ, Horton KA (1994) Distribution of thermal areas on active lava flow field: Landsat observations of Kilauea, Hawaii, July 1991. *Bull Volcanol* 56:284–296
- Flynn LP, Harris AJL, Wright R (2001) Improved identification of volcanic features using Landsat 7 ETM+. *Remote Sens Environ* 78:180–193
- Flynn LP, Wright R, Garbeil H, Harris AJL, Pilger E (2002) A global thermal alert using MODIS: initial results from 2000–2001. *Adv Environ Monit Model* 1:37–69
- Francis PW, Rothery DA (1987) Using the Landsat thematic mapper to detect and monitor active volcanoes: an example from Lascar Volcano, northern Chile. *Geology* 15:614–617
- Gawarecki SJ, Lyon RJP, Nordberg W (1965) Infrared spectral returns and imagery of the Earth from space and their application to geological problems: scientific experiments for manned orbital flight. *Am Astronaut Soc Sci Technol Ser* 4:13–133
- Gouhier M, Harris A, Calvari S, Labazuy P, Guéhenneux Y, Donnadiou F, Valade S (2012) Lava discharge during Etna's January 2011 fire fountain tracked using MSG-SEVIRI. *Bull Volcanol* 74(4):787
- Harris A, Ripepe M (2007) Temperature and dynamics of degassing at Stromboli. *J Geophys Res* 112, B03205. doi:[10.1029/2006JB004393](https://doi.org/10.1029/2006JB004393)
- Harris AJL, Blake S, Rothery DA, Stevens NF (1997) A chronology of the 1991 to 1993 Etna eruption using AVHRR data: implications for real time thermal volcano monitoring. *J Geophys Res* 102:7985–8003
- Harris AJL, Wright R, Flynn LP (1999) Remote monitoring of Mount Erebus Volcano, Antarctica, using polar orbiters: progress and prospects. *Int J Remote Sens* 20(15–16):3051–3071
- Harris AJL et al (2001) Automated, high temporal resolution, thermal analysis of Kilauea volcano, Hawai'i, using GOES satellite data. *Int J Remote Sens* 22(6):945–967
- Kaneko T, Wooster MJ (2005) Satellite thermal analysis of the 1986 Izu-Oshima lava flows. *J Volcanol Geotherm Res* 148:355–371
- Lombardo V, Buongiorno MF (2003) Temperature distribution analysis of July 2001 Mt. Etna eruption observed by the airborne hyperspectral sensor MIVIS. *Ann Geophys* 46(6)

- Lombardo V, Buongiorno MF (2006) Lava flow thermal analysis using three infrared bands of remote-sensing imagery: a study case from Mount Etna 2001 eruption. *Remote Sens Environ* 101(2):141–149
- Lombardo V, Buongiorno MF, Amici S (2006) Characterization of volcanic thermal anomalies by means of sub-pixel temperature distribution analysis. *Bull Volcanol* 68:641–651
- Neri M, Acocella V, Behncke B, Giammanco S, Mazzarini F, Rust D (2011) Structural analysis of the eruptive fissures at Mount Etna (Italy). *Ann Geophys* 54(5):464–479. doi:[10.4401/ag-5332](https://doi.org/10.4401/ag-5332)
- NRC Committee on Earth Science and Applications from Space (2007) Earth science and applications from space: national imperatives for the next decade and beyond. The National Academies Press of the National Research Council (NRC), Washington, DC, 428pp
- Oppenheimer C (1993) Thermal distributions of hot volcanic surfaces constrained using three infrared bands of remote sensing data. *Geophys Res Lett* 20:431–434
- Oppenheimer C, Francis PW (1997) Remote sensing of heat, lava and fumarole emissions from Efta' Ale Volcano, Ethiopia. *Int J Remote Sens* 18:1661–1692
- Oppenheimer C, Yirgu G (2002) Thermal imaging of an active lava lake: Erta 'Ale volcano, Ethiopia. *Int J Remote Sens* 23:4777–4782
- Oppenheimer C, Francis PW, Rothery DA, Carlton RWT, Glaze LS (1993a) Infrared image analysis of volcanic thermal features: Lascar Volcano, Chile 1984–1992. *J Geophys Res* 98:4269–4286
- Oppenheimer C, Rothery DA, Francis PW (1993b) Thermal distribution at fumarole fields: implications for infrared remote sensing of active volcanoes. *J Volcanol Geotherm Res* 55:97–115
- Pergola N, Tramutoli V, Marchese F (2004) Automated detection of thermal features of active volcanoes by means of Infrared AVHRR records. *Remote Sens Environ* 93:311–327
- Pieri D, Abrams M (2004) ASTER watches the world's volcanoes: a new paradigm for volcanological observations from orbit. *J Volcanol Geotherm Res* 135(1–2):13–28
- Pieri D, Abrams M (2005) ASTER observations of thermal precursors to the April 2003 eruption of Chikurachki Volcano, Kurile Islands, Russia. *Remote Sens Environ* 99:84–94
- Pieri DC, Buongiorno MF (1995) Landsat TM observations of Mt. Etna summit crater radiance increases before the 1991–1993 eruption: implications for ASTER observations. *EOS Trans Am Geophys Union* 1995 Fall Meeting, 76, 46, Nov 7/Supplement, F135
- Pieri D, Glaze LS, Abrams MJ (1990) Thermal radiance observations of an active lava flow during the June 1984 eruption of Mount Etna. *Geology* 18:1018–1022
- Ramsey MS, Dehn J (2004) Spaceborne observations of the 2000 Bezymianny, Kamchatka eruption: the integration of high-resolution ASTER data into near real-time monitoring using AVHRR. *J Volcanol Geotherm Res* 135(1–2):127–146
- Realmuto V, Abrams M, Buongiorno MF, Pieri D (1994) The use of multispectral thermal infrared image data to estimate the sulfur dioxide flux from volcanoes: a case study from Mount Etna, Sicily, July 29, 1986. *J Geophys Res* 99(B1):481–488. doi:[10.1029/93JB02062](https://doi.org/10.1029/93JB02062)
- Rothery DA, Francis PW, Wood CA (1988) Volcano monitoring using short wavelength infrared data from satellites. *J Geophys Res* 93:7993–8008
- Simkin T, Kreuger AF (1977) Skylab 4 observation of volcanoes: Part B – summit eruption of Fernandina Caldera, Galapagos Islands, Ecuador. *Skylab Explores the Earth, NASA Spec Publ* 380, pp 171–172
- Simkin T, Siebert L (1994) *Volcanoes of the world: a regional directory, gazetteer, and chronology of volcanism during the last 10,000 years*, 2nd edn. Geoscience Press, Tucson, 368pp
- Solomon SC, Baker VR, Bloxham J, Booth J, Donnellan A, Elachi C, Evans D, Rignot E, Burbank D, Chao BF, Chave A, Gillespie A, Herring T, Jeanloz R, LaBrecque J, Minster B, Pitman WC III, Simons M, Turcotte DL, Zoback ML (2003) Plan for living on a restless planet sets NASA's solid earth agenda. *EOS Trans Am Geophys Union* 84(45):485–491
- Vaughan RG, Hook SJ (2006) Using satellite data to characterize the temporal thermal behavior of an active volcano: Mount St. Helens, WA. *Geophys Res Lett* 33, L20303

- Vaughan RG, Hook SJ, Ramsey MS, Realmuto VJ, Schneider DJ (2005) Monitoring eruptive activity at Mount St. Helens with TIR image data. *Geophys Res Lett* 32(19)
- Vaughan RG, Abrams MJ, Hook SJ, Pieri DC (2007) Satellite observations of new volcanic island in Tonga. *EOS* 88(4):37–41
- Wooster MJ, Rothery DA (1997) Thermal monitoring of Lascar Volcano, Chile using infrared data from the along track scanning radiometer, a 1992–1995 time series. *Bull Volcanol* 58:566–579
- Wooster MJ, Rothery DA (2000) A review of volcano surveillance applications using the ATSR instrument series. *Adv Environ Monit Model* 1(1):3–35
- Wright R, Flynn LP (2003) On the retrieval of lava flow surface temperatures from infrared satellite data. *Geology* 31:893–896
- Wright R, Rothery DA, Blake S, Harris AJL, Pieri DC (1999) Simulating the response of the IEOS Terra ASTER sensor to high temperature volcanic targets. *Geophys Res Lett* 26:1773–1776
- Wright R, Rothery DA, Blake S, Pieri DC (2000) Improved remote sensing estimates of lava flow cooling: a case study of the 1991 to 1993 Mount Etna eruption. *J Geophys Res (Solid Earth)* 105:23681–23694
- Wright R, Flynn L, Garbeil H, Harris A, Pilger E (2004) MODVOLC: near-real-time thermal monitoring of global volcanism. *J Volcanol Geotherm Res* 135:29–49
- Yamaguchi Y, Kahle AB, Tsu H, Kawakami T, Pniel M (1998) Overview of advanced spaceborne thermal emission and reflection radiometer (ASTER). *IEEE Trans Geosci Remote Sens* 36:1062–1071
- URL1: <http://www.volcano.si.edu>
- URL2: <http://vulcani.ingv.it/en/etna.html>
- URL3: <http://noaasis.noaa.gov/NOAASIS/ml/avhrr.html>